

High Resolution Quantitative Lorentz Microscopy

This content has been downloaded from IOPscience. Please scroll down to see the full text.

2015 J. Phys.: Conf. Ser. 644 012026

(<http://iopscience.iop.org/1742-6596/644/1/012026>)

View [the table of contents for this issue](#), or go to the [journal homepage](#) for more

Download details:

IP Address: 130.209.115.82

This content was downloaded on 19/10/2015 at 15:48

Please note that [terms and conditions apply](#).

High Resolution Quantitative Lorentz Microscopy

S McVitie, D McGrouther and M Krajnak

Scottish Universities Physics Alliance, School of Physics and Astronomy, University of Glasgow, Glasgow G12 8QQ UK

stephen.mcvitie@glasgow.ac.uk

Abstract. The advent of aberration corrected transmission electron microscopy has led to considerable improvements in the field of high resolution electron microscopy imaging. In this paper we show how these developments are applied to imaging of magnetic structure in field free or low field conditions. Whilst the capability of increased spatial resolution is demonstrated on magnetic layers with a width of $< 20\text{nm}$ we also consider how a pixelated detector can be used to dramatically increase the efficiency of the detection of the magnetic signal variation in the presence of strong diffraction contrast.

1. Introduction

The study of magnetic materials in the transmission electron microscope has a long and rich history dating back to the 1950s. Imaging of magnetic structure in the TEM comes under the umbrella of methods termed Lorentz microscopy [1]. Quite simply such imaging can be described in terms of the interaction of the electron beam with the magnetic induction through the classical Lorentz force. Lorentz microscopy as a form of phase imaging can also be considered from a quantum mechanical wave-optical approach, although the interpretation is slightly less intuitive. The latter approach is required for any image calculation and incorporation of microscope parameters. A range of methods exist within TEM such as the defocused Fresnel and displaced aperture Foucault which can be used to image domain walls and domains respectively, albeit these are non-linear methods where quantification can be problematic. In scanning TEM the differential phase contrast (DPC) technique provides quantitative induction maps by mapping the displacement of the electron beam on a segmented detector.

In principle Lorentz microscopy can be practiced on any TEM/STEM, although in order to image the magnetic structure the sample requires to be in field free or a low field environment. For the majority of specimens studied this therefore requires the objective lens to be switched off or be weakly excited. As the objective lens is not used for imaging one has to rely on lenses located further from the sample which are less powerful than the objective lens. This means that the resolution attainable in Lorentz microscopy is generally at least one order of magnitude less than that possible with high resolution TEM. The recent advent of commercially available aberration corrected instruments has transformed the capability of (S)TEM and this has been exploited successfully for high resolution imaging [2]. At Glasgow we have pioneered the use of aberration corrected Lorentz STEM with the DPC mode being used to demonstrate sub nanometer resolution in field free/low field conditions [3].

In this paper we highlight the capabilities that have been afforded with the system now installed at Glasgow. Whilst the superior resolution is one of the main factors of the aberration corrected system



we have also explored possibilities of novel detection where the sensitivity of DPC to small deflection angles (phase gradients) has shown extremely promising results.

2. Experimental set up

As stated previously one of the major advances in (S)TEM imaging recently has been the incorporation of aberration correctors and the resulting increase in spatial resolution. At the University of Glasgow we have a JEOL Atomic Resolution Microscope (JEM-ARM200F) equipped with a CEOS (Corrected Electron Optical Systems GmbH) probe corrector for STEM imaging. This system has a cold field emission gun and operates at accelerating voltages of 60, 80 120 and 200 kV. With the objective lens normally excited the field at the sample is around 20000 Oe (2.0 T). As stated in the previous section Lorentz imaging is carried out in low field or field free conditions. This instrument is flexible and we can control the field at the sample from 0 Oe up to the full objective strength. The remanent field of the objective lens when it is switched off is 150 Oe and for many samples we image with this field present. If lower fields are required we have a control system designed at the University of Warwick which can reduce the field at the sample to 0 Oe. Furthermore we can set any field with the objective lens so that we can observe magnetisations processes by simply tilting the sample with the goniometer.

On this instrument we perform DPC imaging with an 8 segment silicon photodiode array detector (supplied by Deben UK Ltd.) comprising a solid quadrant inside a contiguous annular quadrant. Signals from the detector were amplified using the “Superfast” amplifier (Andrew Armit Designs). For full flexibility and real time display of magnetic induction information the 8 detected signals were acquired, mixed and displayed via four Gatan Digiscan II units which mean that up to 16 signal combinations may be displayed simultaneously.

We have also explored DPC imaging with pixelated detectors. Initial experiments were carried out using a CCD camera (Gatan Orius) to record the bright field disk. A CCD camera is not ideally suited for STEM imaging due to issues such as charge spreading and its low frame rate. However here it was used to demonstrate the principle of improving the DPC imaging by recording the diffraction disk at each point in the scan. Subsequently using image processing on this data set allowed an analysis of the beam deflection. The Orius camera has high resolution (11MPix resolution, 4008×2672 pixels) but was binned 4× to reduce the large amount of data associated generated by recording a diffraction images at each point in the scan. The timescale of such imaging was also problematic due to the maximum frame rate of the camera being only 14 Hz. For the imaging carried out here we used a beam dwell time of 50 ms to obtain a 100×100 pixel STEM image, further taking account of the camera readout time the images were acquired over 12 minutes. Realistically such long acquisition times are not practical as both stability and sample drift issues are of considerable concern, particularly if larger image sets are to be taken. To overcome this a direct solid state detector is being investigated which will allow shorter acquisition times. With this in mind we have are looking at a direct radiation pixelated detector known as Medipix3 [4]. This detector is currently being tested and we expect this will result in acquisition times being reduced by at least an order of magnitude.

3. Imaging considerations

DPC imaging has been used to image many magnetic systems producing detailed induction maps to aid our understanding of nanomagnetic structures. However it should be noted that the Lorentz interaction for many thin films results in a very small deflection of the electron beam. As an example consider a uniformly magnetized thin film as shown in Fig. 1(a), the interaction of the electron beam with the thin film results in a magnetic deflection angle, β_L , which can be shown to equal $(e\lambda/h)B_S t$ where B_S is the saturation induction of the material, t is the film thickness. The fundamental constants are the magnitude of electronic charge (e), electron wavelength (λ) and Planck’s constant (h). For reference a typical value for a permalloy ($\text{Ni}_{80}\text{Fe}_{20}$) film with $B_S = 1.0$ T and thickness 10 nm we calculate β_L to be 6.4 μrad . This compares with typical Bragg angles which are 10 mrad or more. In terms of DPC STEM imaging, a schematic of the arrangement is shown in Fig 1(b) where the local

deflection of the beam is detected via a quadrant detector. By taking difference signals from opposite segments of the detector components of the integrated induction can be mapped. A point to note is that only the bright field disk is detected on the quadrant detector.

When the objective lens is switched off in the JEOL-ARM200F the probe angles subtended at the sample are much lower than for HREM being in the range of a few mrad and below. With the probe aberration corrector the optimum probe angle (α) is 3.2 mrad which give a diffraction limited probe size of around 1.5 nm and a resolution half of this value [3]. Whilst this is very high resolution for magnetic imaging it is also important to consider the sensitivity of the technique in being able to measure small deflections. We can consider this in more detail by looking at the lengthscales (spatial frequencies in the detector plane). This is illustrated in Fig 1(c) for the case of an annular split detector comprising two segments, with an electron beam being displaced due to a Lorentz force or phase gradient. In the detector plane we can consider angular quantities or spatial frequencies which we can equate, e.g. $k_\alpha = \alpha/\lambda$. For an optimum probe angle of 3.2 mrad and a 200 kV beam with $\lambda = 2.51$ pm, we have a spatial frequency $k_\alpha = (0.8 \text{ nm})^{-1}$. The important spatial frequencies shown in the figure are the probe radius (k_α), the inner radius of the annulus (k_i) and the spatial frequency associated with the beam deflection (k_β). We should note also that for the typical Lorentz deflection angle given earlier (6.4 μ rad) this corresponds to a very low spatial frequency $k_\beta = (400 \text{ nm})^{-1}$, note that the deflection in the figure is exaggerated. The annular detector is the basis of modified DPC in which it was shown to provide a suppression of the non magnetic signal variation due to differential Bragg scattering from the 5-10 nm diameter crystallites comprising the thin film compared to standard DPC [5]. This filtering of the high spatial frequency signal relative to the low spatial frequency magnetic signal variation becomes more enhanced as the ratio (k_i/k_α) becomes close to unity. It is evident that the spatial frequency associated with the magnetic films is considerably smaller than bright field disk by almost two orders of magnitude. We will discuss this further in the next section. Recently the use of pixelated detectors to record STEM diffraction patterns has allowed a number of advances. These have resulted in making further efficiencies in enhancing the phase information in STEM DPC imaging [6].

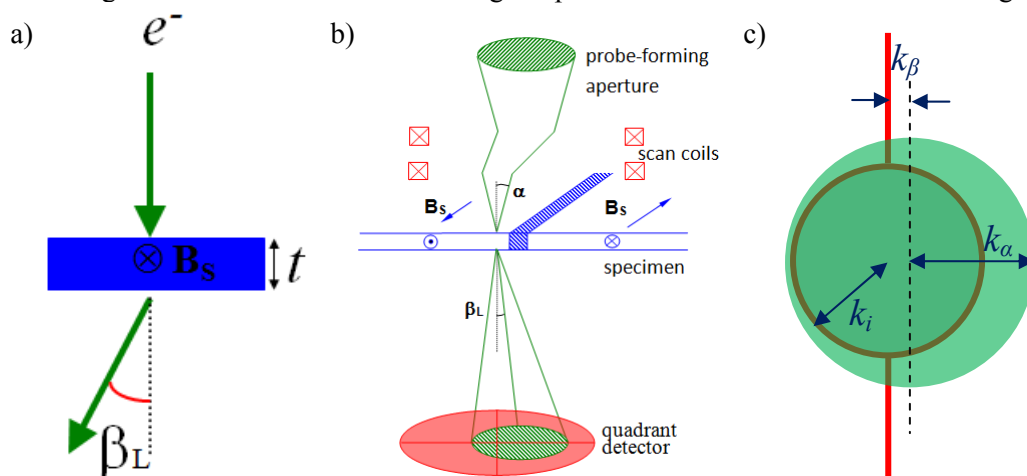


Fig 1. a) Schematic of the deflection of the electron beam from a uniformly magnetised (saturation induction B_s) film of thickness t . b) STEM DPC imaging schematic showing the key quantities of probe angle, α , and the Lorentz deflection, β_L . c) Schematic of bright field disk falling on annular split detector, showing the key quantities in reciprocal space: the probe radius, k_α , magnetic spatial frequency, k_β , and inner detector radius, k_i .

In the following section we demonstrate the resolution improvement capability that has been achieved with the STEM corrector system with an example from a magnetic thin film system possessing nanometer scale magnetic structure. Furthermore we look at the possibilities of improvements for magnetic imaging with pixelated detectors.

4. Results

In this section we present results which demonstrate the possibilities with the aberration correction system. Firstly the capability in terms of improved spatial resolution is considered, before moving on to looking at how pixelated detection opens up potentially huge improvements in DPC imaging.

We illustrate the power of the resolution of the aberration corrected system on an exchange biased sputtered multilayer sample [7]. This sample comprises a structure of ferromagnetic NiFe (permalloy) layers between anti-ferromagnetic FeMn layers with the structure NiFe/(FeMn/NiFe) \times 10 grown on an oxidised Si substrate with a capping layer of 5nm of Ta. The NiFe layers have an average thickness of 16.5 nm and the FeMn layers an average of 12.8 nm, measured from high resolution STEM imaging. Such a structure is too thick for plan view TEM even if the substrate was removed, so for the experiments conducted here a cross-section sample was prepared using focused ion beam methods resulting in a section of \sim 80 nm thickness. Measurements on the initial exchange bias coupling between the AF and FM layers shows hysteretic behaviour in the continuous film sample with the individual layers reversing in steps so that the sample reversed completely in a field of \sim 150 Oe. For the cross-sectioned sample however the magnetic configuration has an additional factor - in effect the cross-sectioning has patterned each FM layer into a nanowire geometry and the fields required to reverse each layer are consequently much higher. Using the JEOL ARM we easily imaged the state of each FM layer, which had a lateral width of $<$ 20nm. Furthermore using the objective lens field we were able to reverse the moment in the layers by tilting the sample with an in-situ field. An example of the configuration of the cross-section partway through the reversal is shown in the DPC image in Fig. 2(a). Here the component of magnetic induction mapped is parallel to the layer interfaces and it can be clearly seen by the black/white contrast that the FM layers are pointing in opposite directions. Furthermore the antiferromagnetic FeMn layers are grey indicating, as expected, no net induction component in these regions. Whilst the magnetic state of each of the 11 layers can be clearly determined to be up or down in the image, there is a significant variation in contrast within each stripe. For such a layered structure sectioned here it would be expected that the magnetisation should be uniform, whilst the DPC contrast suggests it is not. However the contrast variation is a consequence of the granular structure of the film which this gives rise to (unwanted) diffraction contrast in this phase image. This is a significant problem in interpreting magnetic contrast at the smallest scale. A linetrace across the layers shows the magnetic state of the each layer in Fig. 2(b).

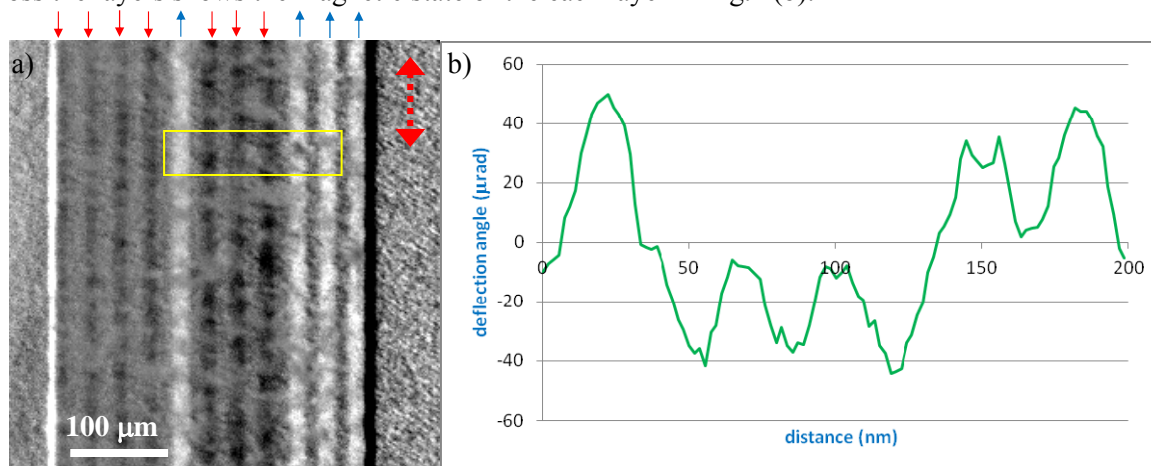


Fig. 2. a) DPC image of exchange biased ferromagnet/antiferromagnet multilayer cross-section. The arrows above the image indicate the direction of magnetisation in the layers and the double headed arrow the direction of sensitivity of the component of magnetic induction. b) Intensity linetrace layers indicated by the yellow box in a) showing the spatial variation of the magnetic induction averaged over this region.

It should be noted we have averaged the signal over a 40 nm width to reduce the effects of diffraction contrast from the granular structure. However even this does not eliminate the effect of

diffraction. The linetrace shows a quantitative signal variation between layers corresponding to a deflection of $\sim \pm 40 \mu\text{rad}$. This is consistent, but slightly less than expected for a material with an integrated induction of $\sim \pm 80 \text{ Tnm}$, corresponding to permalloy with a saturation induction of 1.0 T and film thickness of 80 nm. The transition between the FM and AF layers shows a variation on a lengthscale of the order of 5 nm. Whilst the average linetrace shows the power of the spatial resolution of the aberration corrected system with the standard DPC detection, the variation resulting from the crystallite structure clearly shows some problems in imaging this type of material. We now turn our attention to the developments in detection whereby pixelated detectors allow a major improvement in magnetic imaging by the DPC technique.

The advantages of using a pixelated detector for Lorentz DPC will be illustrated by examining images obtained from a magnetic domain wall in a polycrystalline magnetic thin film. The material studied here is 20 nm thick thermally evaporated permalloy doped with platinum ($\text{Py}_{90}\text{Pt}_{10}$) which has a grain size in the range 5-10 nm. By mapping the integrated induction parallel to the wall we obtain an image of a 180° wall using the standard quadrant detector as shown in Fig. 3(a). It is apparent that there is weak, but visible, underlying black/white contrast within the image corresponding to the large scale magnetic domains. However there is also very high contrast on the 5-10 nm scale resulting from differential Bragg scattering in and between the grains.

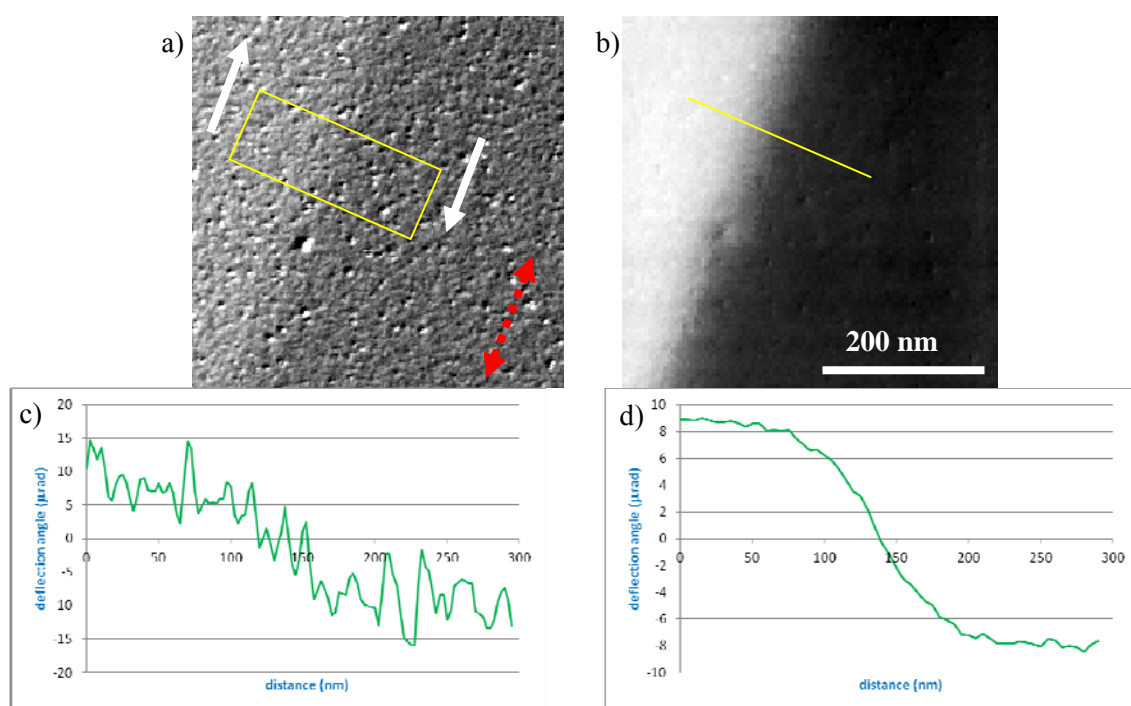


Fig. 3. a) DPC image of 180° domain wall in a 20nm thick platinum doped permalloy film. The arrows indicate the direction of magnetisation in each domain and the double headed arrow the direction of sensitivity of the component of magnetic induction. b) Processed DPC images from a pixelated detector from the same 180° domain wall. c) Intensity linetrace across DPC image of a) averaged over 100 nm of the domain wall as indicated by the yellow box in a). d) Intensity linetrace across DPC image of b) from single line of the domain wall as indicated by the yellow line in a).

When we use the Orius CCD camera to record the bright field disk at each point in the scan we are then able to use image processing to maximize the magnetic phase information that can be extracted. The theory of phase imaging and the contrast functions for DPC imaging are well developed and the theoretical basis is calculated for sinusoidal phase variations being propagated through the electron optical system. The information can be thought of in terms of overlapping disks in the detector plane

[5,6]. In this respect the detector geometry is fundamentally important in terms of any contrast transfer function. The pixelated detector allows considerable flexibility in applying different effective detector geometries to the data sets of the bright field disks. For magnetic imaging using an annular detector which is just smaller than the bright field disk is shown to be very efficient, this is known as modified DPC [5]. This efficiency can be explained simply in that the intensity variations within the bright field disk are mostly associated with the high spatial frequency signal due to the crystallites, by removing this intensity variation this signal is suppressed whilst the signal associated with the beam deflection is preserved. We have found that the most efficient method of removing this variation for the diffraction data set is to use edge detection methods for the bright field disk, which in effect is like having an annular detector just smaller than the disk at each deflection. Put simply this is equivalent to a super efficient modified DPC detector where the ratio k_i/k_a is virtually unity. The improvement in the detected magnetic signal variation is shown Fig. 3(b), where the crystallite signal variation has been massively reduced. Further evidence of the magnitude of the reduction in the signal variation is shown by taking linetraces across the domain wall. For the DPC image the quantitative signal variation based on conversion of the difference signal to a magnetic deflection is shown in Fig. 3(c) with the linetrace for is shown which is averaged over 50 lines. Even this averaging shows a variation associated with the crystallites. By contrast a single line trace across the edge detection processed image is shown on Fig. 3(d). The improvement is quite startling and represents a huge advance in DPC imaging allowing point by point interpretation of magnetic signal variations in polycrystalline films. Whilst the improvement is significant one point of caution must be noted, a quantitative analysis of phase changes where the phase gradient changes rapidly, i.e. at the domain walls needs to be investigated further in order for any quantification to be justified. We will report on current work using the Medipix3 detector in the near future.

5. Conclusions

Aberration corrected DPC STEM offers exciting possibilities for imaging of magnetic materials. The developments in pixelated detection also mean flexible application of the contrast transfer function of the system becomes possible to improving magnetic and more generally phase imaging.

Acknowledgements

We are grateful to colleagues at JEOL, JEOL (UK), Gatan, Deben UK Ltd. and Andrew Armit Designs for their input to the development of the instrument and associated hardware. Additionally we would like to thank Prof R. Bowman and Dr S. O'Reilly for provision of the exchange biased sample, Dr A Hrabec for provision of the PyPt sample and to Mr F. Gonclaves, and Mr W. Smith for cross-section sample preparation. We also acknowledge financial support from the EPSRC (EP/I013520/1), the Scottish Universities Physics Alliance (SUPA), the University of Glasgow and Seagate. The link for open access research data is found here (<http://dx.doi.org/10.5525/gla.researchdata.204>)

References

- [1] Chapman J N 1984 *J. Phys. D. Appl. Phys.* **17** 623
- [2] Krivanek O L, Corbin G J, Dellby N, Elston B F, Keyse R J, Murfitt M F, Own C S, Szilagy Z S and Woodruff J W 2008 *Ultramicroscopy* **108** 179
- [3] McVitie S, McGrouther D, McFadzean S, MacLaren D A, O'Shea K J and Benitez M J 2015 *Ultramicroscopy* **152** 57
- [4] Ballabruga R, Campbell M, Heijne E, Llopart E, Tlustos E and Wong W 2011 *Nucl. Instr. Meth. Phys. Res. A* **633** S15
- [5] Chapman J N, McFadyen I R and McVitie S 1990 *IEEE Trans. Magn.* **26** 1506
- [6] Pennycook T J, Lupini A R, Yang H, Murfitt M F, Jones L and Nellist P D 2015 *Ultramicroscopy* **151** 160
- [7] Hill C B, Hendren W R, Bowman R M, McGeekin P K, Gubbins M A and Venugopal V A 2013 *Meas. Sci. Technol.* **24** 045601